The Astrophysical Journal, 976:190 (12pp), 2024 December 1 https://doi.org/10.3847/1538-4357/ad85e3

Strong Nongravitational Accelerations and the Potential for Misidentification of Near-Earth Objects

Aster G. Taylor[1,9], Darryl Z. Seligman[2,10], Matthew J. Holman[3], Peter Vereš[3], Davide Farnocchia[4], Nikole Lewis[2], Marco Micheli[5], and Jason T. Wright[6,7,8]
[1] Department of Astronomy, University of Michigan, Ann Arbor, MI 48109, USA; agtaylor@umich.edu
[2] Department of Astronomy and Carl Sagan Institute, Cornell University, 122 Sciences Drive, Ithaca, NY 14853, USA
[3] Harvard-Smithsonian Center for Astrophysics, Minor Planet Center, 60 Garden St., Cambridge, MA 02138, USA
[4] Jet Propulsion Laboratory, California Institute of Technology, 4800 Oak Grove Dr., Pasadena, CA 91109, USA
[5] ESA NEO Coordination Centre, Largo Galileo Galilei 1, I-00044 Frascati (RM), Italy
[6] Department of Astronomy & Astrophysics, The Pennsylvania State University, University Park, PA 16802, USA
[7] Center for Exoplanets and Habitable Worlds, The Pennsylvania State University, University Park, PA 16802, USA
[8] Penn State Extraterrestrial Intelligence Center, The Pennsylvania State University, University Park, PA 16802, USA
Received 2024 July 24; revised 2024 September 18; accepted 2024 October 9; published 2024 November 22

Abstract

Nongravitational accelerations in the absence of observed activity have recently been identified on near-Earth objects (NEOs), opening the question of the prevalence of anisotropic mass loss in the near-Earth environment. Motivated by the necessity of nongravitational accelerations to identify 2010 VL_{65} and 2021 UA_{12} as a single object, we investigate the problem of linking separate apparitions in the presence of nongravitational perturbations. We find that nongravitational accelerations on the order of 1×10^{-9} au day^{-2} can lead to a change in plane-of-sky positions of $\sim 1 \times 10^{3}$ arcsec between apparitions. Moreover, we inject synthetic tracklets of hypothetical nongravitationally accelerating NEOs into the Minor Planet Center orbit identification algorithms. We find that at large nongravitational accelerations ($|A_i| \geqslant 1 \times 10^{-8}$ au day^{-2}) these algorithms fail to link a significant fraction of these tracklets. We further show that if orbits can be determined for both apparitions, the tracklets will be linked regardless of nongravitational accelerations, although they may be linked to multiple objects. In order to aid in the identification and linkage of nongravitationally accelerating objects, we propose and test a new methodology to search for unlinked pairs. When applied to the current census of NEOs, we recover the previously identified case but identify no new linkages. We conclude that current linking algorithms are generally robust to nongravitational accelerations, but objects with large nongravitational accelerations may potentially be missed. While current algorithms are well-positioned for the anticipated increase in the census population from future survey missions, it may be possible to find objects with large nongravitational accelerations hidden in isolated tracklet pairs.

Unified Astronomy Thesaurus concepts: Asteroids (72); Celestial mechanics (211); Comets (280); Near-Earth objects (1092)

1. Introduction

It has recently become evident that there exists a continuum of activity in small bodies in the solar system between the traditional definitions of comets and asteroids. Active asteroids (D. Jewitt 2012; H. H. Hsieh 2017; D. Jewitt & H. H. Hsieh 2022) and main belt comets (H. Boehnhardt et al. 1996; E. W. Elst et al. 1996; I. Toth 2000; H. H. Hsieh et al. 2004; H. H. Hsieh & D. Jewitt 2006) are objects on classically asteroid-like orbits that display visible activity in the form of faint comae. There also exist objects on cometary trajectories that appear inactive, such as "Manx comets" (K. J. Meech et al. 2016) and Damocloids (D. J. Asher et al. 1994; D. Jewitt 2005). These intermediate objects could provide critical insights into our understanding of processes such as volatile and organic delivery to terrestrial planets (C. F. Chyba 1990; T. Owen & A. Bar-Nun 1995; F. Albarède 2009), cometary fading (J. H. Wang & R. Brasser 2014; R. Brasser & J. H. Wang 2015), and the depletion of volatiles or mantling on small bodies (M. Podolak & G. Herman 1985; D. Prialnik & A. Bar-Nun 1988).

1I/'Oumuamua was the first interstellar object discovered traversing the inner solar system based on its hyperbolic trajectory (G. V. Williams et al. 2017). It exhibited significant nongravitational acceleration in the radial direction of $A_1 \sim 2.5 \times 10^{-7}$ au day^{-2} (M. Micheli et al. 2018). However, deep optical imaging of the object displayed no dust coma (D. Jewitt et al. 2017; K. J. Meech et al. 2017) or detection of carbon-based species outgassing (Q.-Z. Ye et al. 2017; D. E. Trilling et al. 2018). It is still unclear what mechanism is responsible for 'Oumuamua's nongravitational acceleration, although M. Micheli et al. (2018) concluded that for realistic densities and geometries, outgassing with little or no associated dust production was the most likely cause. While its provenance remains unknown, J. B. Bergner & D. Z. Seligman (2023) proposed that radiolytic production of H_2 from H_2O ice may be responsible for the acceleration. For recent reviews, see A. Fitzsimmons et al. (2023), D. Jewitt & D. Z. Seligman (2023), and D. Z. Seligman & A. Moro-Martín (2022).

S. R. Chesley et al. (2016), D. Farnocchia et al. (2023), and D. Z. Seligman et al. (2023) identified seven near-Earth objects (NEOs) that also exhibited significant nongravitational accelerations and no associated dust coma (the "dark comets"). Moreover, these accelerations were inconsistent with the typical causes of nongravitational acceleration on asteroids,

[9] Fannie and John Hertz Foundation Fellow.
[10] NSF Astronomy and Astrophysics Postdoctoral Fellow.

such as the Yarkovsky effect (D. Vokrouhlický et al. 2015) or radiation pressure (D. Vokrouhlický & A. Milani 2000). Therefore, it was hypothesized that these objects were also outgassing with little dust production (at least when observed), similar to 'Oumuamua and potentially due to seasonal effects (A. G. Taylor et al. 2024a).

A case of particular relevance in this context is that of 2010 VL_{65}.[11] D. Z. Seligman et al. (2023) reported that the orbit of 2010 VL_{65} could be readily linked with that of 2021 UA_{12},[12] but only if an out-of-plane nongravitational acceleration of $A_3 \sim 9 \times 10^{-10}$ au day^{-2} was included in the fit.

These examples show that compositional assumptions and/or the absence of observed activity cannot rule out nongravitational accelerations on objects in the near-Earth environment. Instead, astrometric orbit fitting is necessary to identify nongravitational accelerations for these objects. This methodology requires data over long arcs and several apparitions. If only gravity-only orbits are considered, nongravitational accelerations may disrupt these data arcs by causing objects to be incorrectly identified across apparitions, thereby obscuring nongravitational accelerations in the near-Earth environment.

Motivated by the case of 2010 VL_{65}, we demonstrate that a sufficiently large nongravitational acceleration causes the on-sky position of an object to shift between apparitions in comparison to a gravity-only orbit. We quantify this change in on-sky position from nongravitational perturbations for test cases of dark comets in Section 2, a synthetic population of asteroids in Section 3, and for the currently known NEOs in Section 4. This effect could plausibly lead to linkage failures, which would cause a single object to be falsely identified as distinct objects across apparitions. Therefore, in Section 5, we assess the accuracy of the current Minor Planet Center (MPC) linking algorithms. Informed by these results, in Section 6 we search for unlinked pairs in the current census of NEOs. We discuss our results and their broader ramifications in Section 7.

2. Dark Comet Test Cases

In this section, we present ephemerides of two dark comets (1998 KY_{26} and 2003 RM) under the influence of nongravitational perturbations. These objects are representative members of two distinct populations—2003 RM is large ($R_N \sim 230$ m) and is on an orbit with $a \sim 3$ au and $e \sim 0.6$, while 1998 KY_{26} has $R_N \sim 15$ m, $a \sim 1.2$ au, and $e \sim 0.2$.

We use the `ASSIST` code (M. J. Holman et al. 2023), which is an extension of the `REBOUND` N-body code (H. Rein & S. F. Liu 2012) and the `REBOUNDx` library (D. Tamayo et al. 2020). `ASSIST` integrates test particles with the IAS15 integrator (H. Rein & D. S. Spiegel 2015), using precomputed positions of the Sun, Moon, planets, and 16 massive asteroids with the JPL DE441 ephemeris (D. Farnocchia 2021; R. S. Park et al. 2021). As a result, `ASSIST` is significantly more efficient than a classic N-body integrator at the precision needed for ephemerides, at least in a solar system context.

The `ASSIST` package can incorporate nongravitational accelerations using the B. G. Marsden et al. (1973) formulation, which we implement in this paper. Specifically, the nongravitational acceleration takes the form

$$\boldsymbol{a}_{\rm NG} = (A_1\hat{\boldsymbol{r}} + A_2\hat{\boldsymbol{t}} + A_3\hat{\boldsymbol{n}})\, g(r). \quad (1)$$

In Equation (1), the $g(r)$ function captures the dependence of the H_2O activity on the heliocentric distance r. We set $g(r) = (r_0/r)^2$, where $r_0 = 1$ au. The unit vectors $\hat{\boldsymbol{r}}$, $\hat{\boldsymbol{t}}$, and $\hat{\boldsymbol{n}}$ correspond to the radial, transverse, and out-of-plane directions with respect to the object's Keplerian orbit. The free parameters A_1, A_2, and A_3 provide the magnitude of the corresponding component of the nongravitational acceleration.

We integrate the trajectories of 2003 RM and 1998 KY_{26} with a range of nongravitational accelerations in order to quantify the change in on-sky position. These simulations are initialized on 2000 January 1 and integrated for 50 yr. For each object, we add a nongravitational acceleration in the form of Equation (1). We consider each component direction separately and a range of magnitudes of nongravitational acceleration. For each nongravitational acceleration and direction, we calculate the change in the on-sky position $\Delta\Theta$ relative to the trajectory with the same initial conditions and gravity-only motion. The change in position $\Delta\Theta$ is defined to be the offset angle between the on-sky positions of each trajectory. If the geocentric direction vector is $\boldsymbol{n}_{\rm GO}$ on a gravity-only trajectory and $\boldsymbol{n}_{\rm NG}$ on a nongravitationally accelerating trajectory, then the difference in on-sky position is

$$\Delta\Theta = \cos^{-1}(\boldsymbol{n}_0 \cdot \boldsymbol{n}_{\rm NG}). \quad (2)$$

Larger values of the $\Delta\Theta$ parameter correspond to larger discrepancies between the predicted (gravity-only) position and the perturbed on-sky position of the object. This could lead to misidentification of objects across apparitions—a new observation may be categorized as a previously unidentified object rather than as an apparition of an already known object.

In Figure 1, we show the change in on-sky position for all three directions of nongravitational acceleration for 2003 RM and 1998 KY_{26}. We only show the orbits for a nongravitational acceleration magnitude of $|A_i| = 1 \times 10^{-10}$ au day^{-2}, but the small magnitudes of nongravitational acceleration means that $\Delta\Theta$ is a linear function of acceleration magnitude (D. Farnocchia et al. 2015). This is only the case if the nongravitational acceleration is small compared to the gravitational acceleration due to the Sun, which takes the form of $A_1 = -3 \times 10^{-4}$ au day^{-2} at 1 au. In addition, if an object has a close encounter with a planet, then the ephemerides will no longer be linear. Due to the dynamically chaotic environment, differences in position from nongravitational accelerations will lead to significant differences in the trajectories.

It is evident that the nongravitational accelerations can drive significant changes in the on-sky position of both objects —$\Delta\Theta \gtrsim 10''$—over timescales comparable to the orbital period and apparition timescale. Moreover, the transverse nongravitational acceleration A_2 is far more efficient at modulating the sky position than the other component directions. This is consistent with expectations—A_2 causes residuals to grow quadratically in time, A_1 causes residuals to grow linearly in time, and A_3 is not cumulative.

Note that the changes in on-sky position shown in Figure 1 vary periodically in time in addition to the expected growth. The change in position peaks during close approaches to Earth, since $\Delta\Theta \propto d^{-2}$, where d is the distance between the observer and the object. The object is brightest and most likely to be observed during these close approaches. In addition, smaller objects are dimmer and are more likely to be observed only

[11] https://ssd.jpl.nasa.gov/tools/sbdb_lookup.html#/?sstr=2010vl65
[12] https://ssd.jpl.nasa.gov/tools/sbdb_lookup.html#/?sstr=2021ua12

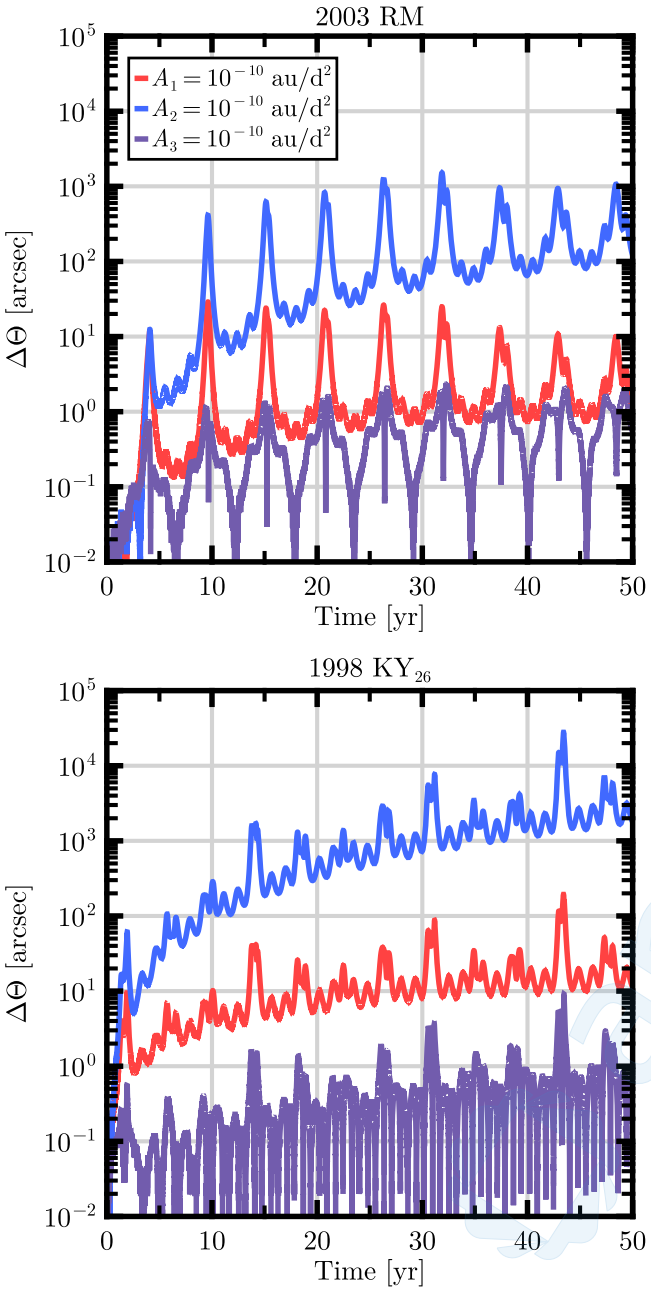

Figure 1. The change in the on-sky position (as seen from Earth) of 2003 RM (top) and 1998 KY_{26} (bottom) as a function of time for the three components of nongravitational acceleration. The magnitude of the nongravitational acceleration is set to $|A_i| = 1 \times 10^{-10}$ au day^{-2} and we show the radial A_1 (red), transverse A_2 (blue), and out-of-plane A_3 (purple) components. Since the ephemerides are linear in the nongravitational acceleration magnitude, stronger accelerations have the same functional form. The nongravitational accelerations are of the form given in Equation (1), and the change in position $\Delta\Theta$ between the perturbed and unperturbed orbits is calculated using Equation (2).

during close approaches, when the changes in on-sky position are more significant.

3. Synthetic Population

In this section, we generalize the results from Section 2 to arbitrary orbits and accelerations. We repeat our analysis of ephemerides on a synthetic population that spans the orbits of NEOs.

This synthetic population consists of 1×10^5 objects with orbital elements drawn from uniform distributions. Specifically, objects in the population are drawn with semimajor axis $a \in [0.5, 4.2)$ au, eccentricity $e \in [0, 1)$, inclination $i \in [0, 15)°$, argument of perihelion $\omega \in [0, 360)°$, longitude of ascending node $\Omega \in [0, 360)°$, and true anomaly at epoch $f_0 \in [0, 360)°$. We then add nongravitational accelerations to each object and calculate the change in on-sky position relative to gravity-only orbits. We consider each of the directions of nongravitational acceleration and with magnitudes logarithmic-uniformly sampled from $|A_i| \in [1 \times 10^{-12}, 1 \times 10^{-7}]$ au day^{-2}. After integrating for 1 and 10 yr, we calculate the changes in on-sky position.

In Figure 2, we show the median changes in position after 10 yr of integration time under a transverse nongravitational acceleration versus semimajor axis and eccentricity. This component is shown because it produces the largest changes in on-sky position (see Section 2). Analogous calculations for (i) the radial and out-of-plane directions and (ii) shorter integration times are shown in Figures A1–A5 in the Appendix. While A_2 generates the largest change in position, it is evident from Figures A1–A5 that radial and out-of-plane accelerations can also drive significant changes in position in some cases, even over shorter 1 yr timescales.

4. Application to NEO Population

In this section, we perform the same calculation as in Sections 2 and 3 for all currently known NEOs. For each NEO in the JPL Small-Body Database,[13] we calculate the change in on-sky position for a general nongravitational acceleration. Each NEO is given a nongravitational acceleration with a magnitude of $|A_i| = 1 \times 10^{-10}$ au day^{-2} in each component direction. Each object is initialized at its orbital position when it was first discovered, and then integrated for an approximate apparition period. The apparition period is assumed to be approximately the larger of (i) the object's orbital period and (ii) the maximum gap between subsequent observations. The observational times are obtained from the MPC Small Bodies Database.[14]

After a single apparition period, we calculate the distance between the object's on-sky position with and without nongravitational accelerations. For a set magnitude and direction of the nongravitational acceleration, we calculate the fraction of all NEOS with corresponding changes in on-sky position greater than a specified cutoff after an apparition. Although the integration is only performed for a single nongravitational acceleration magnitude, we scale the ephemerides by this magnitude, since we assume that the ephemerides are linear (Section 2). We show these fractions in Figure 3.

Relatively weak nongravitational accelerations ($|A_2| \sim 1 \times 10^{-9}$ au day^{-2}) can produce degree-scale changes in on-sky position in $\gtrsim$1% of NEOs (Figure 3). This result should not be interpreted to mean that nongravitational accelerations exist on the calculated fraction of NEOs. Instead, these calculations are intended to suggest that NEOs with sufficiently strong nongravitational accelerations may have large changes in on-sky position.

[13] https://ssd.jpl.nasa.gov/tools/sbdb_lookup.html
[14] https://www.minorplanetcenter.net/data

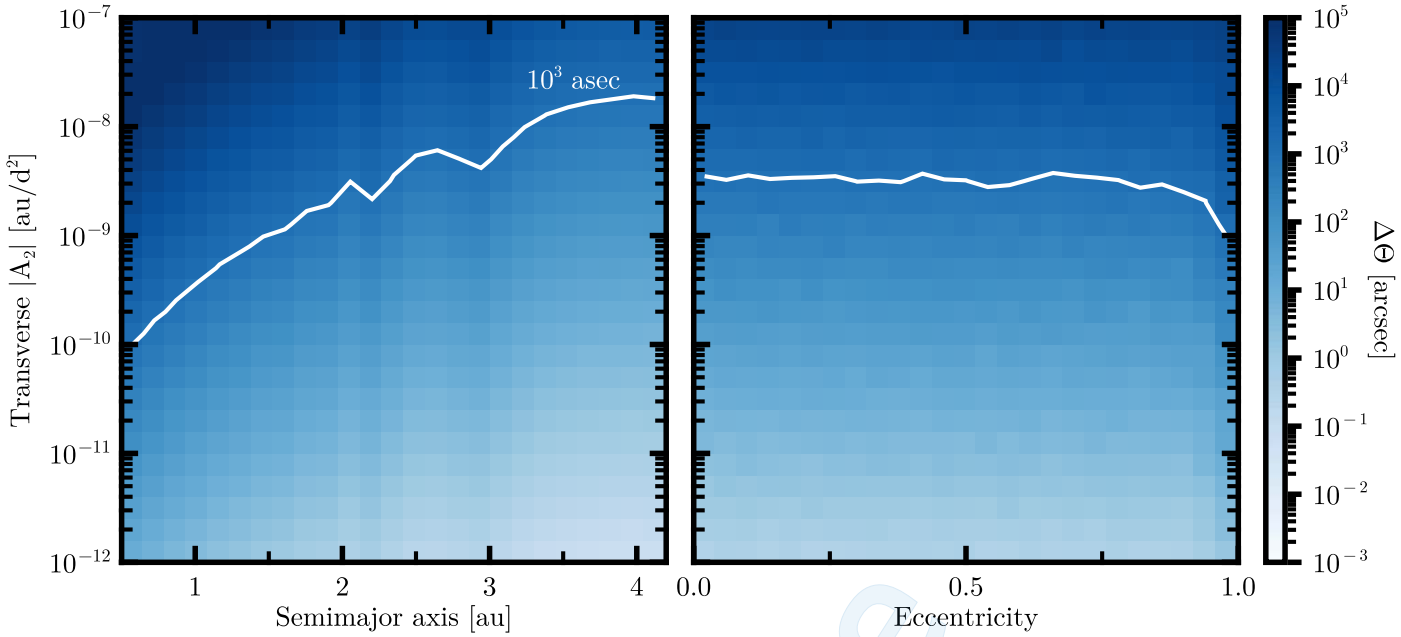

Figure 2. The median change in the on-sky position $\Delta\Theta$ after 10 yr of integration as a function of the magnitude of the transverse nongravitational acceleration A_2, semimajor axis, and eccentricity. Each grid cell shows the median change in position of all objects in a given bin. The white contour corresponds to $\Delta\Theta = 10^3$ arcsec.

5. Fidelity of the MPC Linking Algorithm

In this section, we present a preliminary proof-of-concept assessment of the fidelity of the MPC linking algorithm for NEOs with significant nongravitational accelerations. While the MPC also relies on user-reported linkages, the algorithms used by observers are varied and not publicly available. As a result, we only assess the fidelity of the MPC's internal orbit fitting and linkage pipeline. A detailed assessment of the capabilities of linking algorithms—considering a comprehensive variety of nongravitational accelerations, orbits, apparition spacing, and observation spacing—is warranted but is outside the scope of this paper.

The algorithm to link observations across apparitions has two principal components—attribution and identification. In the attribution process, novel astrometric observations are directly attributed to previously known orbits. If the attribution process fails, it is still possible to link apparitions through the identification process. Once sufficient observations are made in the new apparition, a second orbit can be calculated and identified as an extension of a known orbit. We consider both of these processes independently, but note that both are used to link objects.

5.1. Orbit Attribution

The internal MPC attribution algorithm has two components —`checkid` and `s9m`. The `checkid` algorithm takes the orbits of currently known objects and performs a simple Keplerian advance to the date of the new data. It then calculates (i) the offset of the data from the predicted on-sky position and (ii) the change in the mean anomaly required to correct this offset. The `s9m` algorithm first reduces a given tracklet to the first and last observations contained within it. The position of the reduced tracklet is then compared to the predicted positions of the orbits of all previously identified objects. In contrast to `checkid`, the `s9m` algorithm propagates the fully perturbed orbits to the tracklet observations, although nongravitational accelerations are not included. An object with a planetary close encounter between apparitions would be linked by `s9m`, but not by `checkid`. A linkage is made if (i) a previously identified orbit is within the search radius of 2″ and (ii) the on-sky velocity vectors of both objects are aligned.

We assess the linkage fidelity of both of these algorithms for objects with a range of magnitudes and directions of nongravitational acceleration. The sample contains 1000 currently known NEOs that have multiple apparitions separated by less than 15 yr.[15] For each object, we generate synthetic observations across an apparition. The temporal spacing between apparitions is assumed to be the maximum separation between observations in current data. We first generate a short data arc, which consists of two observations separated by 1 hr on the 1st, 6th and 12th nights (six in total). The position of the object at the first observation time is obtained from the JPL Solar Systems Dynamics' Horizons System.[16] The positions at all other times are generated by numerical integration with `ASSIST`. We generate a tracklet at the subsequent apparition, which consists of two observations separated by 1 hr for two nights, for a total of four observations. While such evenly spaced observations are unrealistic, the observation spacing is kept constant for all objects. Therefore, the (generally dominant; A. Milani & G. F. Gronchi 2010) errors from observation spacing are roughly constant for the different trajectories.

For each NEO, we generate tracklets with (i) a gravity-only orbit and (ii) logarithmically spaced nongravitational accelerations in each component direction and magnitudes ranging from 1×10^{-12} au day^{-2} to 1×10^{-7} au day^{-2} (19 tracklets in total for each object). Each synthetic observation accounts for the light travel time and reports the geocentric R.A., decl., and apparent magnitude. Object apparent magnitudes are computed following the magnitude law for asteroids[17] (not shown) with

[15] The second criterion is imposed for the sake of computational efficiency.
[16] https://ssd.jpl.nasa.gov/horizons/
[17] Minor Planet Circular 10193.

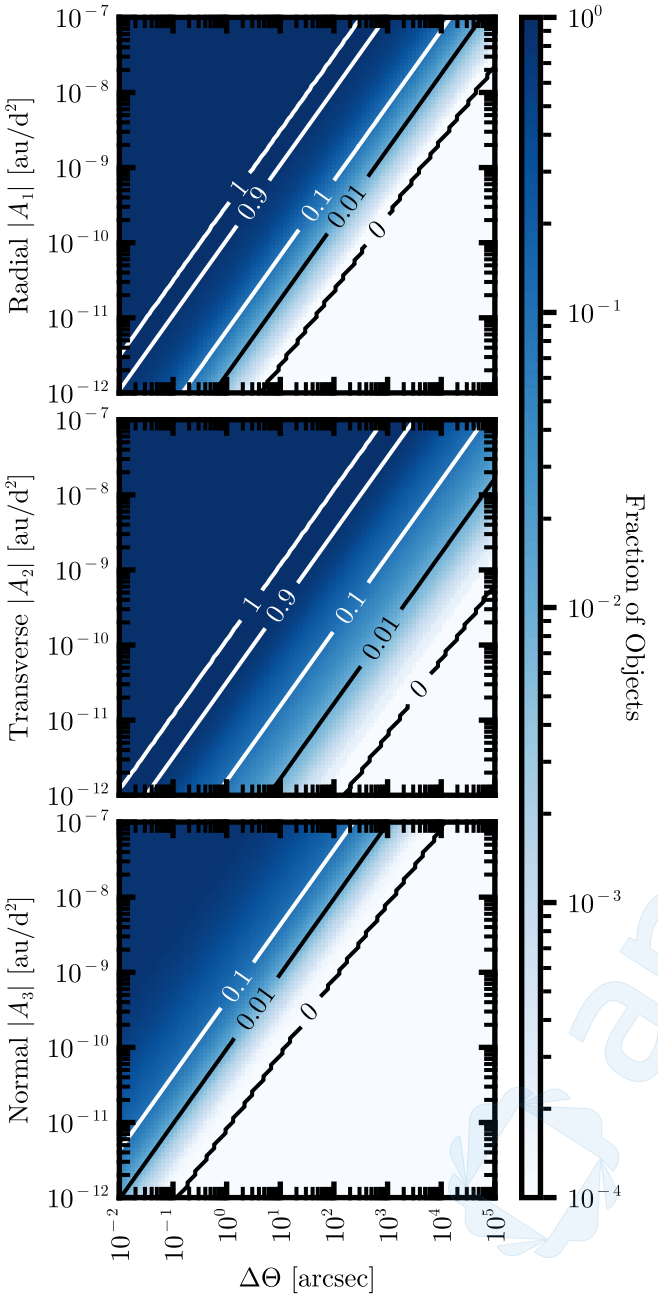

Figure 3. The fraction of NEOs that would exhibit a given change in sky position (or larger) over an approximate apparition period as a function of magnitude and direction of nongravitational acceleration. The ephemerides are calculated for $|A_i| = 1 \times 10^{-10}$ au day^{-2} and linearly scaled for other nongravitational acceleration magnitudes.

the absolute magnitude H given by the JPL Small-Body Database and slope $G = 0.15$, typical for asteroids.

We assess the fidelity with which the current MPC pipeline can link these synthetic tracklets to prior short-arc observations as a function of magnitude and direction of nongravitational acceleration. Due to the relatively sparse synthetic data, only $N_{\rm GO} = 379$ of the 1000 gravity-only tracklets are successfully linked to their original objects by either `checkid` or `s9m`. We calculate the number of tracklets $N_{\rm NG}$ that are successfully linked to prior short-arc data for each magnitude and direction of nongravitational acceleration. In Table 1, we report $N_{\rm NG}/N_{\rm GO}$, the fraction of nongravitationally accelerating tracklets that are successfully linked across apparitions, relative to gravity-only trajectories.

Table 1
Linkage Fraction

$\lvert A_i\rvert$ (au day^{-2})	Radial	Transverse	Normal
10^{-12}	0.9974	0.9947	1.0
10^{-11}	0.9974	0.9921	1.0026
10^{-10}	0.9921	0.9815	0.9974
10^{-9}	0.9868	0.9288	1.0106
10^{-8}	0.9525	0.3826	0.9736
10^{-7}	0.7467	0.0106	0.2876

Note. Values shown are the fractions of synthetic tracklets (relative to gravity-only tracklets) that are successfully linked by the MPC linkage algorithm for a given magnitude and direction of nongravitational acceleration.

The linkage fraction is greater than 1 for some out-of-plane nongravitational accelerations. This occurs because fitting an orbit to a tracklet is a slightly random process that depends on the precise on-sky position. At low acceleration magnitudes, out-of-plane nongravitational accelerations produce small changes in the on-sky position of a tracklet. These variations are not sufficient to cause a linkage failure but will induce small random variations in the orbit fitting to the tracklet. A few objects whose gravity-only tracklets failed orbit fits will be successfully fit and linked once nongravitational accelerations are included, leading to fractions that are slightly greater than 1. This does not indicate that nongravitational accelerations improve the linkage process, but that the linkage process is inherently stochastic.

Successful linkage fractions significantly decrease in the presence of nongravitational accelerations with magnitudes larger than those identified for dark comets ($\gtrsim 1 \times 10^{-9}$ au day^{-2}). Transverse nongravitational accelerations cause the sharpest decline in linkage fraction, and only ∼90% of tracklets with a magnitude of transverse acceleration of $A_2 \sim 1 \times 10^{-9}$ au day^{-2} are successfully linked. At a magnitude of nongravitational acceleration of $A_2 \sim 1 \times 10^{-7}$ au day^{-2}, the linked fraction drops to ∼1%.

While there is no known mechanism to produce such large transverse nongravitational accelerations (besides cometary outgassing), these results show that objects with these accelerations would be difficult to link and detect. However, radial nongravitational accelerations of this magnitude are known to exist and cause linkage failures in ∼25% of the considered objects. Therefore, it is possible that hypothetical NEOs with large nongravitational accelerations would not be correctly attributed across apparitions.

5.2. Orbit Identification

It is still possible to link apparitions via orbit identification if attribution fails. If a sufficient number of observations are obtained during a new apparition, an independent orbit can be computed. These newly computed orbital elements are then compared to previously known orbits. If the two sets of orbital elements are within 3σ of each other, then the apparitions are linked. In this subsection, we test the fidelity of this process in the presence of nongravitational accelerations. Specifically, we test whether nongravitational accelerations can cause a previously successful linkage to fail.

We construct a sample of 214 NEOs that were successfully recovered across multiple apparitions from the MPC data set. For each object, we identify the first apparition and record the times of each subsequent observation. We then calculate synthetic trajectories with a range of nongravitational accelerations and record the geocentric R.A. and decl. at each observation time. Orbits are then individually determined for both the first and second apparitions and the two sets of orbital elements are compared. The two apparitions are considered successfully linked if the two sets of orbital elements are separated by $<3\sigma$.

The fraction of orbits that are successfully linked (generally $\sim$80%) is independent of the magnitude of the nongravitational acceleration, so nongravitational accelerations do not induce a linkage failure. However, nongravitational accelerations cause issues in the orbit identification process. For sufficiently large nongravitational accelerations (generally $A \sim 1 \times 10^{-6}$ au day^{-2}), the initial orbit determination will consistently fail, especially for long-arc data. This will prevent accurate linkage, since short-arc data will still be consistent with a gravity-only orbit.

Moreover, the perturbations from nongravitational accelerations within each apparition tend to increase the uncertainty in the orbital elements calculated. In fact, the uncertainties for nongravitationally accelerating orbits can be larger than the uncertainties for a gravity-only orbit by an order of magnitude or more. Since the orbit identification process uses a 3σ criterion, these large uncertainties increase the probability of a correct linkage. However, in this test we only compare the apparitions of already-linked known objects, and ignore extraneous linkages to alternative objects. In a realistic scenario, an orbit fit to a new apparition will be compared to all previously identified orbits. In this case, the larger uncertainties make it more likely that more than one previously known object will be linked to the new apparition, confusing the identification.

Even once a multiple linkage occurs, more observations will continue to refine the estimates of orbital parameters. As the uncertainty shrinks, possible linkages will be pruned away until only one remains. However, the nongravitational accelerations will have modified the orbital parameters between apparitions. If the uncertainties shrink quickly, then it is possible that a multiply-linked object will become unlinked and registered as a new object. This is likely what occurred for 2010 VL$_{65}$. While false linkages to a large number of objects are possible, objects with the large nongravitational accelerations necessary to produce this effect will be rare and are unlikely to dramatically affect the NEO census.

6. Search for Unlinked NEOs

In this section, we search for unlinked pairs within the current census of NEOs. We consider (i) the orbital angular momentum, (ii) the orbital elements, and (iii) novel constants of motion (derived in Section 6.1) as metrics to link pairs of NEOs. While these metrics do not identify any unlinked pairs in the current NEO population, they may be useful for linking objects with nongravitational accelerations in future observations or between isolated tracklets.

6.1. Constants of Motion under the Action of Nongravitational Accelerations

In this subsection, we derive quantities that are conserved under the action of nongravitational acceleration for a two-body system. These quantities provide a potentially useful metric for identifying unlinked pairs in the NEO population.

Consider an orbit characterized by the set of Keplerian orbital elements $\boldsymbol{x} = [a, e, i, \Omega, \omega, M_0]$. Under the action of nongravitational accelerations, these will have an orbit-averaged rate of change $\dot{\boldsymbol{x}}$. We wish to find a scalar function $F(\boldsymbol{x})$ that is constant over the trajectories defined by $\dot{\boldsymbol{x}}$. Equivalently, the trajectories must be isosurfaces of F, or $\dot{\boldsymbol{x}} \cdot \nabla F = 0$.

The rate of change of this phase-space position is given by

$$\dot{\boldsymbol{x}} = \frac{hr_0^2}{\mu a^2 \eta} \begin{bmatrix} 2A_2 a/\eta^2 \\ A_2(1-\eta)/e \\ -A_3 \cos\omega(1-\eta)/(e\eta) \\ -A_3 \csc i \sin\omega(1-\eta)/(e\eta) \\ A_3 \cot i \sin\omega(1-\eta)/(e\eta) \\ -2A_1. \end{bmatrix}. \tag{3}$$

The quantity η is defined to be $\eta = \sqrt{1-e^2}$. Equation (3) is derived by averaging the Gauss planetary equations (C. D. Murray & S. F. Dermott 2000) over a single orbital period, assuming that the parameters do not change significantly over the period, or equivalently that the magnitude of the nongravitational acceleration is small. We additionally assume that the radial dependence of the nongravitational acceleration is $g(r) \propto r^{-2}$, although analogous equations can be derived for a generic radial dependence. A derivation of these equations can be found in Appendix A.3 of A. G. Taylor et al. (2024a). Our requirement that $\dot{\boldsymbol{x}} \cdot \nabla F = 0$ becomes

$$\begin{aligned} 0 = &\frac{2a}{\eta^2} A_2 \frac{\partial F}{\partial a} + \frac{1-\eta}{e} A_2 \frac{\partial F}{\partial e} \\ &- \frac{1-\eta}{e\eta} \cos\omega A_3 \frac{\partial F}{\partial i} - \frac{1-\eta}{e\eta} \frac{\sin\omega}{\sin i} A_3 \frac{\partial F}{\partial \Omega} \\ &+ \frac{1-\eta}{e\eta} \cot i \sin\omega A_3 \frac{\partial F}{\partial \omega} - 2A_1 \frac{\partial F}{\partial M_0}. \end{aligned} \tag{4}$$

We require that Equation (4) is satisfied for any orbital parameters and that F does not depend on A_1, A_2, or A_3. In order to ensure that Equation (4) holds for all values of A_i, we can divide F into several functions U, V, and W such that

$$0 = \frac{2a}{\eta^2} A_2 \frac{\partial U}{\partial a} + \frac{1-\eta}{e} A_2 \frac{\partial U}{\partial e}, \tag{5a}$$

$$\begin{aligned} 0 = &-\frac{1-\eta}{e\eta^2} \cos\omega A_3 \frac{\partial V}{\partial i} - \frac{1-\eta}{e\eta} \frac{\sin\omega}{\sin i} A_3 \frac{\partial V}{\partial \Omega} \\ &+ \frac{1-\eta}{e\eta} \cot i \sin\omega A_3 \frac{\partial V}{\partial \omega}, \text{ and} \end{aligned} \tag{5b}$$

$$0 = -2A_1 \frac{\partial W}{\partial M_0}. \tag{5c}$$

We will solve each in turn.

Equation (5a) can be solved by separation of variables to find that

$$U(a, e) = \ln\left[\frac{(\eta-1)^2}{a\eta^2}\right]. \tag{6}$$

Note that any arbitrary differentiable function $\boldsymbol{c}_1(U)$ is also a constant of motion.

Dividing Equation (5b) by $(1-\eta)A_3/(e\eta^2)$, we are left with the equation

$$0 = \cos\omega\frac{\partial V}{\partial i} + \sin\omega\csc i\frac{\partial V}{\partial \Omega} - \cot i\sin\omega\frac{\partial V}{\partial \omega}. \quad (7)$$

This equation is not immediately separable. However, none of the terms depend on Ω. As a result, we separate $V(i, \Omega, \omega) = G(i, \omega)K(\Omega)$. For a constant λ, we find that

$$K(\Omega) = \exp(-\lambda\Omega) \quad (8a)$$

$$\lambda G(i, \omega) = \sin i\cot\omega\frac{\partial G}{\partial i} - \cos i\frac{\partial G}{\partial \omega}. \quad (8b)$$

Equation (8b) can further be solved to find that

$$G(i, \omega) = \boldsymbol{c}_2(2\sin i\sin\omega) \times \exp(-\lambda\arctan(\cos i\tan\omega)), \quad (9)$$

where $\boldsymbol{c}_2$ is an arbitrary differentiable function. We select $\boldsymbol{c}_2(x) = \exp(x)$, set $\lambda = -1$, and note that $V(i, \Omega, \omega) = \boldsymbol{c}_3(K(\Omega)G(i, \omega))$. Taking $\boldsymbol{c}_3(x) = \ln(x)$, we find that

$$V(i, \Omega, \omega) = 2\sin i\sin\omega + \arctan(\cos i\tan\omega) + \Omega. \quad (10)$$

The motion of a given object in orbital parameter space is constrained to follow isosurfaces of Equations (6) and (10). Isosurfaces of the U parameter are one-dimensional curves that will be followed precisely. However, isosurfaces of the V parameter are two-dimensional manifolds, so the phase-space trajectory is not immediately given.

The solution to Equation (5c) is trivial—$W(M_0) = c$, where c is a constant. This implies that no constant of motion can be constructed that depends on the mean anomaly at epoch M_0.

It is hypothetically possible to define another (linearly independent) scalar function $Q(i, \Omega, \omega)$ that is also a constant under nongravitational accelerations, which would provide the trajectory. However, if such a function exists, it must be the case that $\dot{\boldsymbol{x}} \cdot \nabla Q = 0$. Since ∇V and ∇Q are both orthogonal to $\dot{\boldsymbol{x}}$, if Q exists we must be able to define Q and V such that $\nabla V \times \nabla Q = \dot{\boldsymbol{x}}$. However, it can be shown that $\nabla \cdot (\nabla V \times \nabla Q) = 0$ for all V, Q, while $\nabla \cdot \dot{\boldsymbol{x}} = -\cot i\cos\omega \neq 0$. Therefore, while we have found a function V, no scalar function Q exists.[18]

The values of the U and V parameters are shown in Figure 4. For the U parameter, the contours of motion are also shown.

In order to verify that these quantities are conserved, we numerically integrated test particles using `REBOUNDx` (D. Tamayo et al. 2020) for a variety of orbital parameters and calculated the value of the U and V parameters over time. For nongravitational accelerations small enough that the orbit-averaged equations of motion hold,[19] the U and V parameters are conserved to machine precision. In the presence of the planets, however, the orbital elements can be subjected to periodic oscillation due to secular perturbations. As a result, a single object may exhibit oscillations in these parameters, although these oscillations are only of magnitude 1×10^{-4}.

[18] It is possible to construct a scalar pseudodensity function ρ such that $\nabla \cdot (\rho\,\dot{\boldsymbol{x}}) = 0$. Such a function enables the construction of V and Q such that $\nabla V \times \nabla Q = \rho\,\dot{\boldsymbol{x}}$. However, there is no closed-form expression for ρ, so it cannot be used to construct useful constants of motion.

[19] This is typically the case when $|A| \lesssim 1 \times 10^{-6}$ au day^{-2} for NEOs, although there is a weak dependence on the orbital period.

6.2. Search Algorithms for Unlinked Pairs

In this subsection, we use the constants of motion derived in Section 6.1, the orbital angular momentum, and the orbital elements to search for unlinked pairs in the current census of NEOs. Specifically, we calculate each quantity for each object in the MPC population of currently known NEOs described in Section 4. For each quantity, we construct a k-dimensional tree for the data and extract the nearest neighbor in the N-dimensional parameter space. In Figure 5, we show histograms of the distance to the nearest neighbor for each NEO in the total population.

We then obtained the closest 0.1% of nearest-neighbor pairs for each parameter set. We used a least-squares fitting method to determine whether these objects could be linked by a nongravitational acceleration (see D. Farnocchia et al. 2015 for a more thorough description of the orbit-fitting algorithm). This methodology was able to recover the previously identified case for 2010 VL_{65} and 2021 UA_{12}, which were identified as a pair by all comparison metrics. Although we recovered many potential pairs of unlinked objects, orbital fitting through object pairs did not recover a single linkage, even when accounting for possible nongravitational accelerations. We therefore conclude that each of these pairs are two distinct objects, with the exception of the previously identified 2010 VL_{65}.

We also tested the accuracy of this methodology for finding linked pairs. We added clones of each object in the current population of NEOs with varying levels of nongravitational acceleration and integrated for one orbital period. We assume that the nongravitational accelerations are sufficiently small that the change in orbital parameters is in the linear regime. We then calculated the fraction of the cloned objects that are the nearest neighbor of the original object in the k-dimensional tree. For sufficiently large nongravitational accelerations, the cloned objects are distinct enough from the original that nearest-neighbor searches will not correctly match these objects. We find that the accuracy of these methods scales with the dimensionality of the parameter under consideration—a higher number of dimensions improves identification of the objects. Regardless, at a magnitude of 1×10^{-6} au day^{-2}, only 88% of cloned objects are linked by comparing orbital parameters. Therefore, more than 1 in 10 clones are nearer to another object than to their original. For an acceleration with magnitude 1×10^{-7} au day^{-2}, 99% of cloned objects are correctly identified. Our search for pairs by orbital parameter implies that there are few, if any, unlinked pairs of NEOs with nongravitational accelerations below this magnitude. However, the assumption of linearity begins to break down for nongravitational accelerations of order 1×10^{-6} au day^{-2} (when the acceleration is greater than 1% of the solar acceleration). As a result, hypothetical objects with stronger nongravitational accelerations would not be identified with the methodology presented in this section, although such objects are expected to be rare.

7. Discussion

In this paper, we demonstrated that nongravitational accelerations can significantly alter the on-sky positions of small bodies. Specifically, we showed that accelerations with magnitudes comparable to or greater than those measured on the currently known dark comets produce changes in on-sky position of $\Delta\Theta \sim 1 \times 10^3$ arcsec over apparition timescales of 1–10 yr. However, we showed that the algorithms currently in use for fitting orbits and linking objects across apparitions are generally robust in the presence of nongravitational

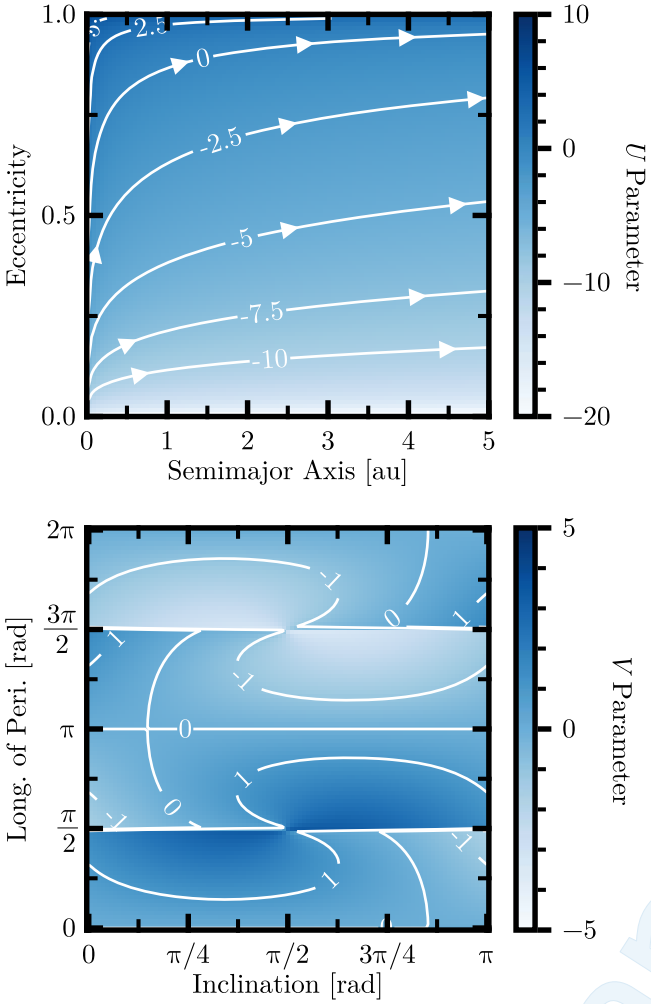

Figure 4. The U parameter (Equation (6)) over a range of (a, e) values and the V parameter (Equation (10)) over a range of (i, ω) values (we set $\Omega = 0$). Contours are shown for both functions. For the U parameter, the contours trace the phase-space trajectories of these objects, which is not the case for the V parameter. In the top panel, the arrows indicate the direction of motion for positive A_2. The contours shown in the bottom panel are not equivalent to the phase-space trajectories.

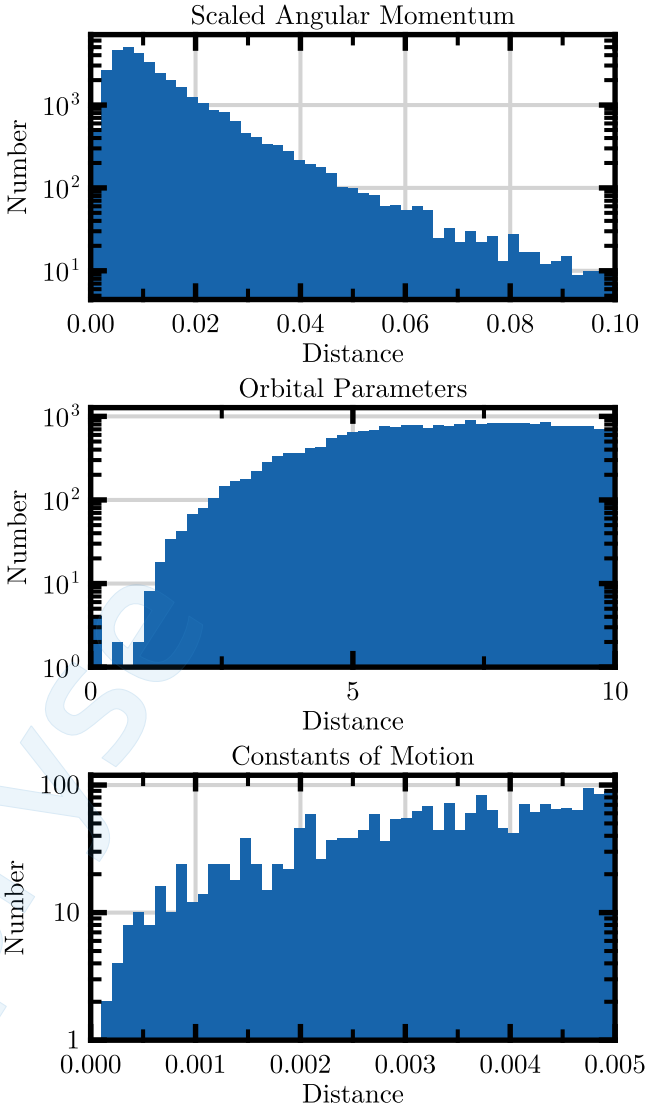

Figure 5. Histograms of the nearest-neighbor distance in orbital angular momentum (top), orbital elements (middle), and the constants of motion given by Equations (6) and (10) (bottom).

accelerations of reasonable magnitude, although objects with large nongravitational accelerations ($|A_i| \gtrsim 1 \times 10^{-8}$ au day^{-2}) may be missed. While accelerations of such magnitude are expected to be rare, our results show that NEOs with such a nongravitational acceleration would be difficult to identify. Therefore, this population is not necessarily well-characterized and may be more common than currently anticipated.

Notably, ∼73% of NEOs in the MPC database have data arcs that are less than a year, and ∼55% have data arcs shorter than a month. In Section 3, we demonstrated that for nongravitational accelerations stronger than those of dark comets by an order of magnitude, ∼10% of NEOs are offset from their predicted on-sky location by more than a degree. Note that this difference is in comparison to a precisely known gravity-only orbit, while actual astrometric positions will include nongravitational accelerations. As a result, the calculated orbits will have errors that may compensate for the residual from nongravitational acceleration, weakening the linkage error.

In Section 5, we investigated the fidelity of the linking algorithm currently in use at the MPC. This process has two principal steps—attribution and identification. In the attribution step, new observations are compared to the expected locations of previously known objects. If the objects are sufficiently close, then the new observations are attributed to the prior object. We determined that transverse nongravitational accelerations an order of magnitude larger than those of the dark comets could lead to an attribution failure rate of ∼10%. However, there are several caveats to this assessment. Our sample is restricted to objects with long data arcs observed across at least one apparition, and only ∼30% of objects could be successfully linked even in the absence of nongravitational accelerations. In addition, objects with transverse nongravitational accelerations with magnitudes $|A_2| \geqslant 1 \times 10^{-8}$ au day^{-2} are hypothetical with no known production mechanism. However, radial nongravitational accelerations of magnitude $|A_1| \simeq 1 \times 10^{-7}$ au day^{-1}, which are possible on comets, can cause linkage failure for ∼25% of considered objects.

Even if an object is not correctly attributed, a linkage can still be made by the orbit identification process. Further observations are collected until a second orbit can be calculated. If these orbital elements are within 3σ of a previously known orbit, then a linkage is made. We found that the orbit identification process

is robust to nongravitational accelerations, as it begins to fail only when gravity-only orbits cannot be calculated for the object's trajectory. In the presence of nongravitational accelerations, however, successful orbit identification is primarily driven not by the similarity in orbital parameters but by the large magnitudes of the uncertainties, which are significantly increased by nongravitational perturbations. As a result, many objects may fall within the 3σ cutoff and be linked to the new apparition, confusing the identification. This complication will likely be exacerbated as the census of solar system small bodies expands. Further investigation is required to determine the significance and prevalence of these issues.

In addition to the changes in on-sky position induced by nongravitational accelerations, trajectories will have aleatory uncertainties as the result of short data arcs (A. Milani & G. F. Gronchi 2010). Such aleatory uncertainties in the ephemerides can often be larger than the uncertainties induced by nongravitational accelerations, contributing to the problem of linking observations. In this work, we compare successful linkages between gravity-only and nongravitationally accelerating trajectories, keeping observation times and data arcs constant. Therefore, our results control for these aleatory effects and depend only on the nongravitational accelerations. While a full investigation of the combined effects of aleatory and epistemic errors in linking is worthwhile, it is beyond the scope of this work.

We also searched for unlinked object pairs using three metrics that should be approximately conserved across apparitions (Section 6). Although we successfully recovered previously linked objects, we did not identify any new unlinked pairs. However, a more rigorous search is warranted, given that larger nongravitational accelerations may cause our pair-identification metrics to fail.

These NEO-pair metrics may be used to identify smaller-magnitude nongravitational accelerations with future observations. Forthcoming observatories such as the the Vera C. Rubin Observatory Legacy Survey of Space and Time (M. E. Schwamb et al. 2023) and NEO Surveyor (A. K. Mainzer et al. 2015; E. L. Wright et al. 2021; A. Mainzer et al. 2022) will expand the census of these objects. With an increased population of NEOs, it may be important to account for nongravitational accelerations when linking objects across apparitions. Moreover, these surveys will also discover smaller objects, which exhibit stronger nongravitational accelerations per unit mass-loss rate than large objects. In addition, smaller objects are dimmer and are more likely to be observed only during close approaches, when the changes in on-sky position are more significant. Therefore, accounting for such nongravitational accelerations may modify the census of NEOs produced by these surveys and identify more volatile-rich bodies in the near-Earth environment. It may also be possible to identify large nongravitational accelerations by mining the Isolated Tracklet File for unlinked observations using the methods discussed in Section 6.

A larger population of hydrated small bodies in the near-Earth environment could have ramifications for current theories of the delivery of terrestrial volatiles. The Earth's water content is generally expected to have been delivered, at least in part, by hydrated small bodies from the outer solar system instead of accretion in situ (K. J. Walsh et al. 2011; D. P. O'Brien et al. 2014; S. N. Raymond et al. 2014). The Earth's isotopic deuterium to hydrogen ratio (D/H; among other isotopic ratios) is significantly higher than that of the protosolar nebula, but significantly lower than that of the long-period or Jupiter-family comets that were once thought to be the source of Earth's oceans (T. Owen & A. Bar-Nun 1995; K. Meech & S. N. Raymond 2020). While main belt comets match the D/H ratio relatively well (C. M. O. Alexander et al. 2012; B. Marty 2012; L. J. Hallis et al. 2015), the origins of terrestrial water remain uncertain. For a more detailed review of the origins of Earth's water, see K. Meech & S. N. Raymond (2020). If the NEO population contains more hydrated objects than anticipated, as suggested by the dark comets, these objects may have contributed to this delivery process. The likely origin of the dark comets in the inner main belt further suggests that volatiles may be common in the near-Earth environment (A. G. Taylor et al. 2024b). Our results imply that it is possible (but unlikely) that more volatile-rich NEOs may exist, but remain undetected due to failures in linkage algorithms.

Moreover, if the future census multiply-counts objects and fails to account for nongravitational accelerations, then orbit predictions and Earth-impact probabilities may be flawed. Since NEOs are the primary source of Earth impactors (R. G. Strom et al. 2005), accounting for nongravitational accelerations may be necessary to fully understand the near-Earth environment and possible future impacts. Specifically, it is possible that undetected nongravitational accelerations could cause a seemingly innocuous NEO to become an Earth impactor. Therefore, our results may have significant implications for both planetary defense and the delivery of volatiles to terrestrial planets. In the context of the upcoming expansion of the census of known NEOs, correctly accounting for nongravitational accelerations may be critical for accurate orbital predictions.

Our results require significant future work to further characterize the issues discussed here. Since the MPC relies heavily on observers to fit orbits and link objects, a survey of the accuracy of current and future linkage methodologies (i.e., HelioLinC; M. J. Holman et al. 2018) is warranted. The tests of the MPC linkage algorithms presented here are limited in scope and only intended to probe a variety of possible issues. Further quantification of the prevalence and severity of possible linking problems is necessary to clarify this issue. Although the MPC's current algorithms appear robust, the future inclusion of nongravitational accelerations in NEO linkage algorithms may overcome these problems and provide a more complete understanding of nongravitational accelerations in the near-Earth environment.

Acknowledgments

We thank the anonymous reviewer for their helpful comments. We thank Paul Abell, Adina Feinstein, Linda Glaser, Megan Mansfield, Luis Salazar Manzano, Robert Jedicke, Ken Chambers, Karen Meech, W. Garrett Levine, Jonathan Lunine, Samantha Trumbo, and Jonathan Williams for useful discussions. A.G.T. acknowledges support by the Fannie and John Hertz Foundation and the University of Michigan's Rackham Merit Fellowship Program. D.Z.S. is supported by an NSF Astronomy and Astrophysics Postdoctoral Fellowship under award AST-2303553. This research award is partially funded by a generous gift of Charles Simonyi to the NSF Division of Astronomical Sciences. The award is made in recognition of significant contributions to Rubin Observatory's Legacy Survey of Space and Time. Part of this research was carried out at the Jet Propulsion Laboratory, California Institute of Technology, under a contract with the National Aeronautics and Space Administration (80NM0018D0004). The Center for Exoplanets and

Habitable Worlds and the Penn State Extraterrestrial Intelligence Center are supported by Penn State and its Eberly College of Science.

This paper made use of the Julia programming language (J. Bezanson et al. 2017), the plotting package Makie (S. Danisch & J. Krumbiegel 2021), the *N*-body code REBOUND (H. Rein & S. F. Liu 2012), and the ephemerides-quality integrator ASSIST (M. J. Holman et al. 2023). This research has made use of data and/or services provided by the International Astronomical Union's Minor Planet Center.

Appendix
Supplemental Material

In this appendix, we show the changes in on-sky position for the synthetic population described in Section 3 for a range of integration times and directions of nongravitational acceleration. Figures A1 and A2 show the changes in on-sky position for radial and out-of-plane accelerations respectively, while Figures A3, A4, and A5 show the radial, transverse, and out-of-plane accelerations (respectively) for an integration period of one year.

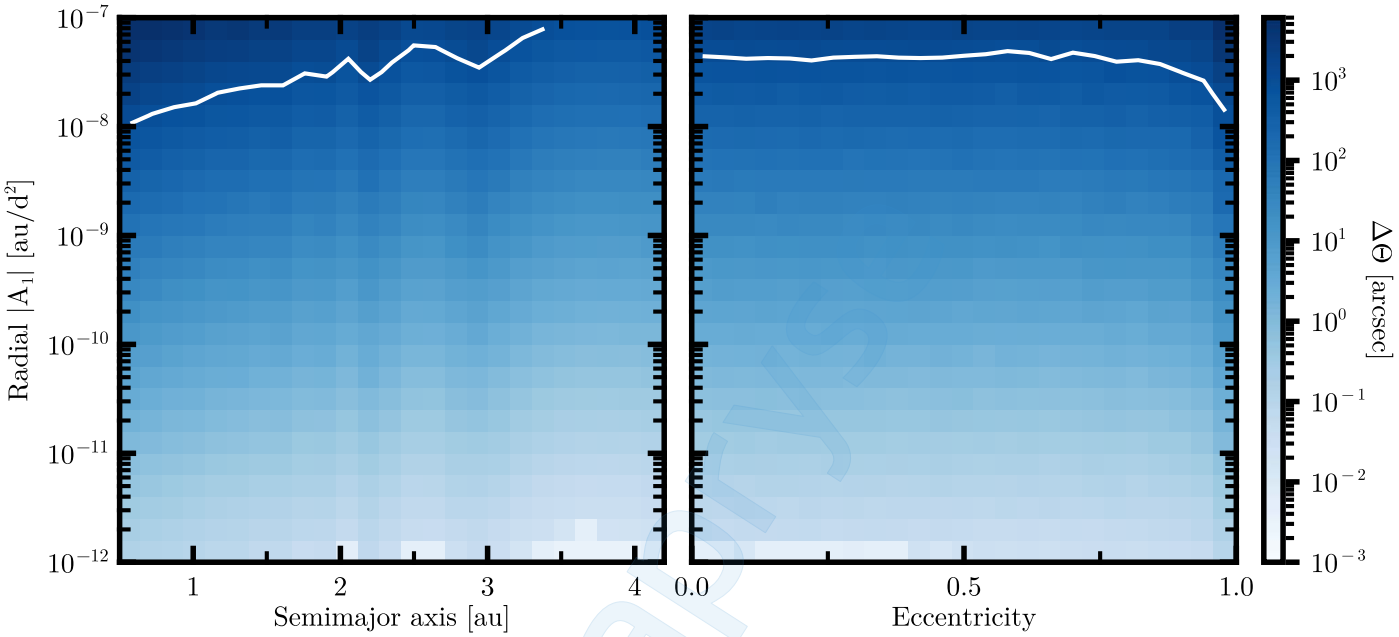

Figure A1. Similar to Figure 2, but with radial A_1 acceleration instead of transverse A_2 acceleration. The contour is at 1×10^3 arcsec.

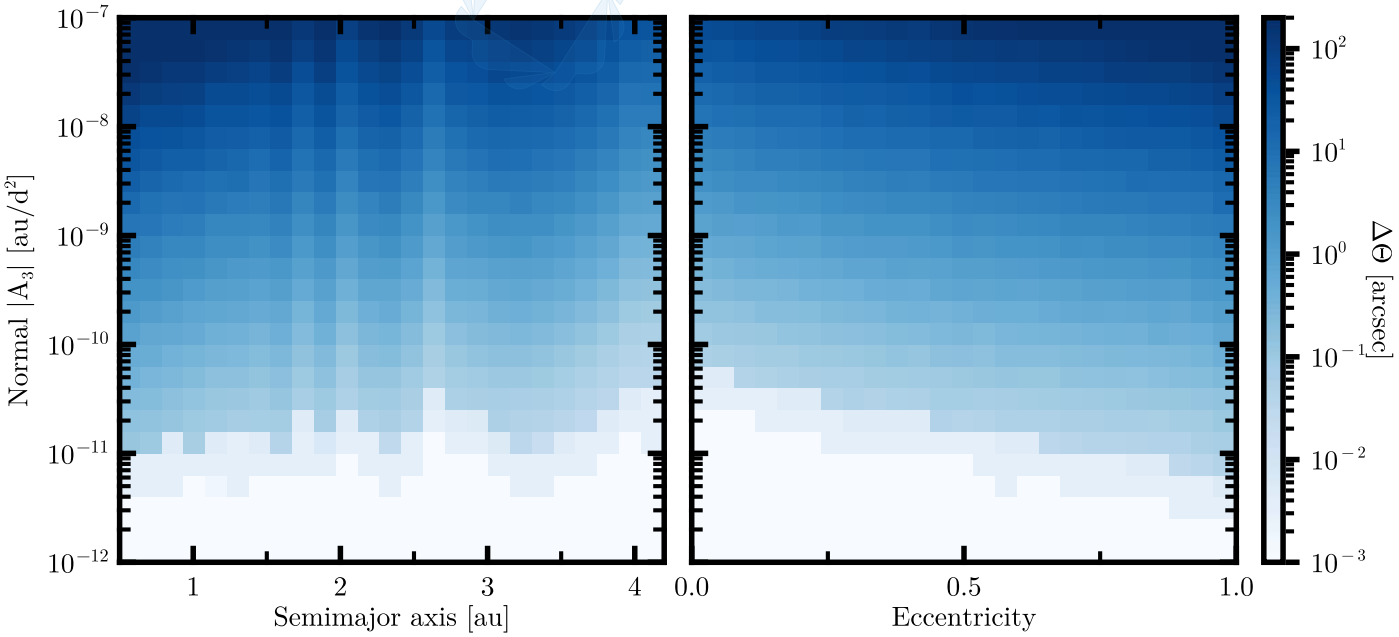

Figure A2. Similar to Figure 2, but with out-of-plane A_3 acceleration instead of transverse A_2 acceleration.

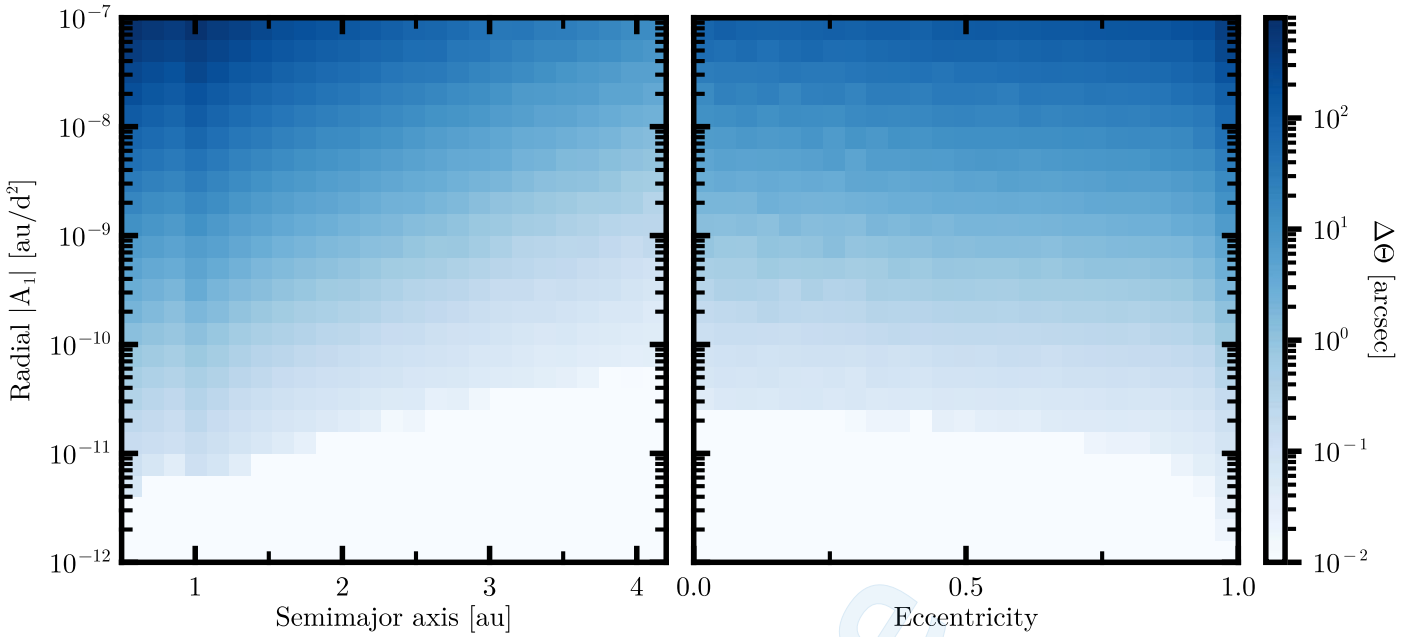

Figure A3. Similar to Figure 2, but with radial A_1 acceleration and an apparition difference of 1 yr.

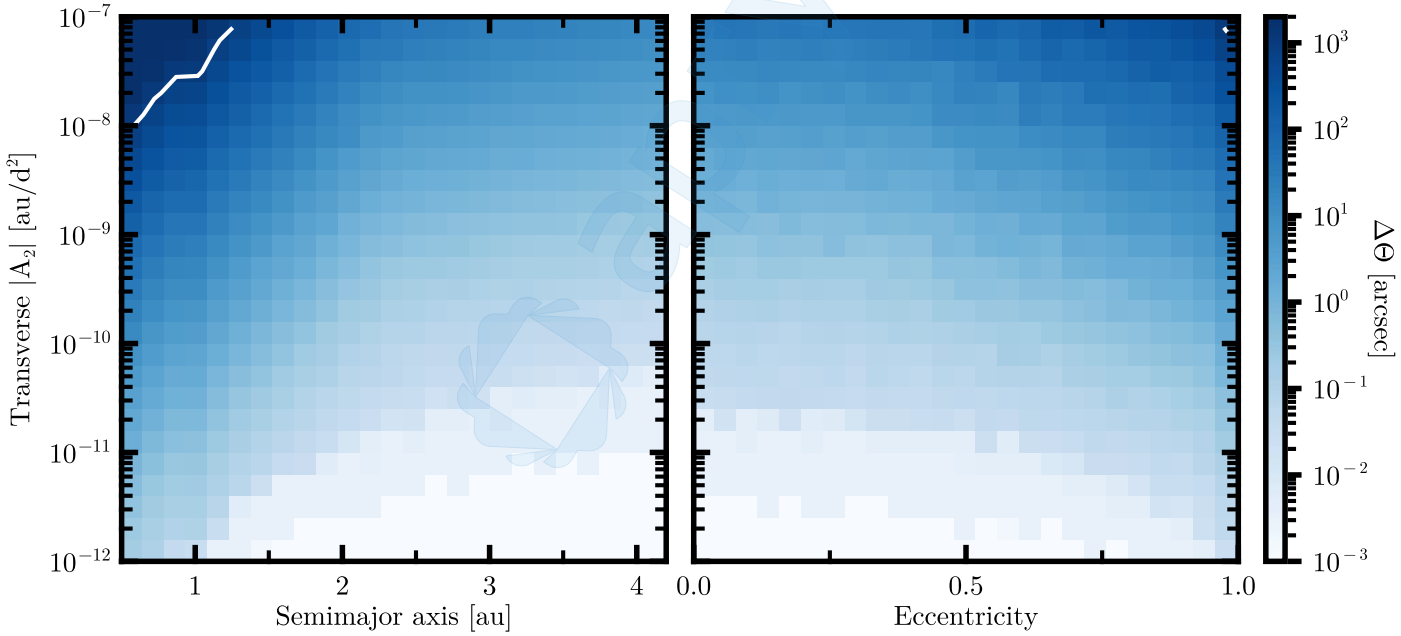

Figure A4. Similar to Figure 2, but for an apparition difference of 1 yr. The contour is at 1×10^3 arcsec.

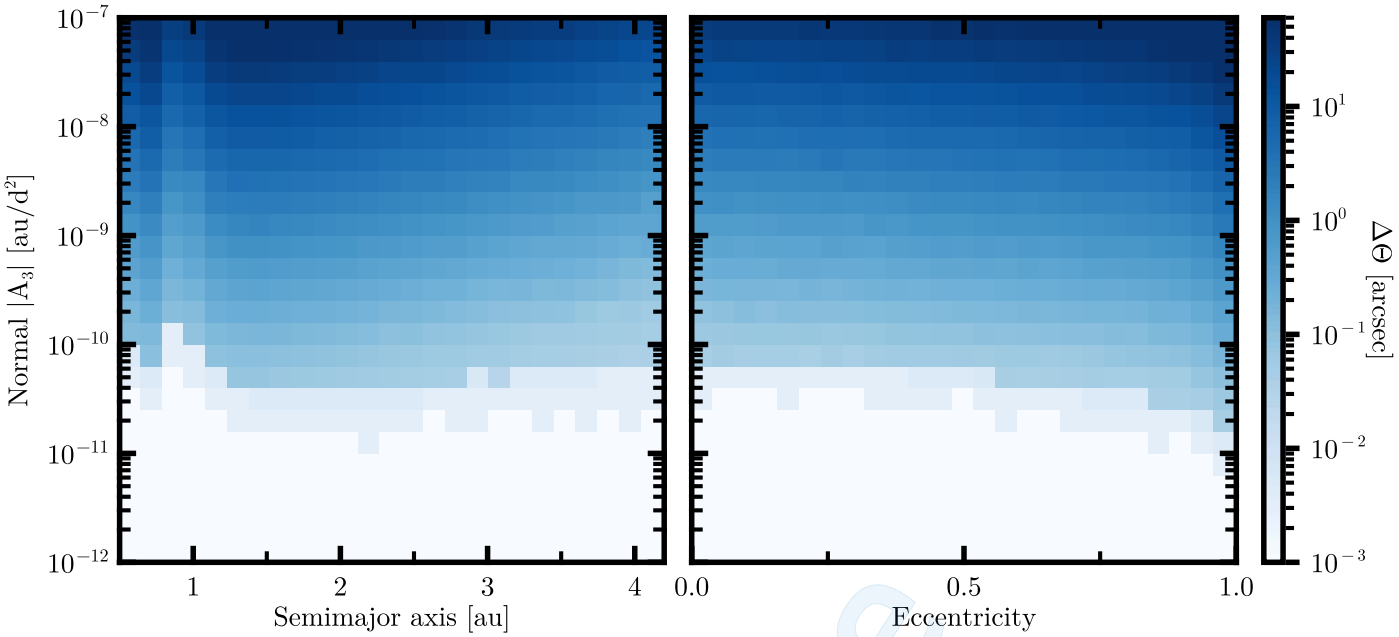

Figure A5. Similar to Figure 2, but with out-of-plane A_3 acceleration and an apparition difference of 1 yr.

ORCID iDs

Aster G. Taylor https://orcid.org/0000-0002-0140-4475
Darryl Z. Seligman https://orcid.org/0000-0002-0726-6480
Matthew J. Holman https://orcid.org/0000-0002-1139-4880
Peter Vereš https://orcid.org/0000-0002-5396-946X
Davide Farnocchia https://orcid.org/0000-0003-0774-884X
Nikole Lewis https://orcid.org/0000-0002-8507-1304
Marco Micheli https://orcid.org/0000-0001-7895-8209
Jason T. Wright https://orcid.org/0000-0001-6160-5888

References

Albarède, F. 2009, Natur, 461, 1227
Alexander, C. M. O., Bowden, R., Fogel, M. L., et al. 2012, Sci, 337, 721
Asher, D. J., Bailey, M. E., Hahn, G., & Steel, D. I. 1994, MNRAS, 267, 26
Bergner, J. B., & Seligman, D. Z. 2023, Natur, 615, 610
Bezanson, J., Edelman, A., Karpinski, S., & Shah, V. B. 2017, SIAMR, 59, 65
Boehnhardt, H., Schulz, R., Tozzi, G. P., Rauer, H., & Sekanina, Z. 1996, IAUC, 6495, 2
Brasser, R., & Wang, J. H. 2015, A&A, 573, A102
Chesley, S. R., Farnocchia, D., Pravec, P., & Vokrouhlický, D. 2016, in IAU Symp. 318, Asteroids: New Observations, New Models, ed. S. R. Chesley et al. (Cambridge: Cambridge Univ. Press), 250
Chyba, C. F. 1990, Natur, 343, 129
Danisch, S., & Krumbiegel, J. 2021, JOSS, 6, 3349
Elst, E. W., Pizarro, O., Pollas, C., et al. 1996, IAUC, 6456, 1
Farnocchia, D. 2021, Small-Body Perturber Files SB441-N16 and SB441-N343, Memorandum, Jet Propulsion Laboratory, https://ssd.jpl.nasa.gov/ftp/eph/small_bodies/asteroids_de441/SB441_IOM392R-21-005_perturbers.pdf
Farnocchia, D., Chesley, S. R., Milani, A., Gronchi, G. F., & Chodas, P. W. 2015, in Asteroids IV, ed. P. Michel et al. (Tucson, AZ: Univ. Arizona Press), 815
Farnocchia, D., Seligman, D. Z., Granvik, M., et al. 2023, PSJ, 4, 29
Fitzsimmons, A., Meech, K., Matrà, L., & Pfalzner, S. 2023, arXiv:2303.17980
Hallis, L. J., Huss, G. R., Nagashima, K., et al. 2015, Sci, 350, 795
Holman, M. J., Akmal, A., Farnocchia, D., et al. 2023, PSJ, 4, 69
Holman, M. J., Payne, M. J., Blankley, P., Janssen, R., & Kuindersma, S. 2018, AJ, 156, 135
Hsieh, H. H. 2017, RSPTA, 375, 20160259
Hsieh, H. H., & Jewitt, D. 2006, Sci, 312, 561
Hsieh, H. H., Jewitt, D. C., & Fernández, Y. R. 2004, AJ, 127, 2997
Jewitt, D. 2005, AJ, 129, 530
Jewitt, D. 2012, AJ, 143, 66
Jewitt, D., & Hsieh, H. H. 2022, arXiv:2203.01397
Jewitt, D., Luu, J., Rajagopal, J., et al. 2017, ApJL, 850, L36
Jewitt, D., & Seligman, D. Z. 2023, ARA&A, 61, 197
Mainzer, A., Masiero, J., Wright, E., et al. 2022, AAS/DPS Meeting, 54, 409.02
Mainzer, A. K., Wright, E. L., Bauer, J., et al. 2015, AAS/DPS Meeting, 47, 308.01
Marsden, B. G., Sekanina, Z., & Yeomans, D. K. 1973, AJ, 78, 211
Marty, B. 2012, E&PSL, 313, 56
Meech, K., & Raymond, S. N. 2020, in Planetary Astrobiology, ed. V. S. Meadows et al. (Tucson, AZ: Univ. Arizona Press), 325
Meech, K. J., Weryk, R., Micheli, M., et al. 2017, Natur, 552, 378
Meech, K. J., Yang, B., Kleyna, J., et al. 2016, SciA, 2, e1600038
Micheli, M., Farnocchia, D., Meech, K. J., et al. 2018, Natur, 559, 223
Milani, A., & Gronchi, G. F. 2010, Theory of Orbital Determination (Cambridge: Cambridge Univ. Press)
Murray, C. D., & Dermott, S. F. 2000, Solar System Dynamics (Cambridge: Cambridge Univ. Press)
O'Brien, D. P., Walsh, K. J., Morbidelli, A., Raymond, S. N., & Mandell, A. M. 2014, Icar, 239, 74
Owen, T., & Bar-Nun, A. 1995, Icar, 116, 215
Park, R. S., Folkner, W. M., Williams, J. G., & Boggs, D. H. 2021, AJ, 161, 105
Podolak, M., & Herman, G. 1985, Icar, 61, 267
Prialnik, D., & Bar-Nun, A. 1988, Icar, 74, 272
Raymond, S. N., Kokubo, E., Morbidelli, A., Morishima, R., & Walsh, K. J. 2014, in Protostars and Planets VI, ed. H. Beuther et al. (Tucson, AZ: Univ. Arizona Press), 595
Rein, H., & Liu, S. F. 2012, A&A, 537, A128
Rein, H., & Spiegel, D. S. 2015, MNRAS, 446, 1424
Schwamb, M. E., Jones, R. L., Yoachim, P., et al. 2023, ApJS, 266, 22
Seligman, D. Z., & Moro-Martín, A. 2022, ConPh, 63, 200
Seligman, D. Z., Farnocchia, D., Micheli, M., et al. 2023, PSJ, 4, 35
Strom, R. G., Malhotra, R., Ito, T., Yoshida, F., & Kring, D. A. 2005, Sci, 309, 1847
Tamayo, D., Rein, H., Shi, P., & Hernandez, D. M. 2020, MNRAS, 491, 2885
Taylor, A. G., Farnocchia, D., Vokrouhlický, D., et al. 2024a, Icar, 408, 115822
Taylor, A. G., Steckloff, J. K., Seligman, D. Z., et al. 2024b, Icar, 420, 116207
Toth, I. 2000, A&A, 360, 375
Trilling, D. E., Mommert, M., Hora, J. L., et al. 2018, AJ, 156, 261
Vokrouhlický, D., Bottke, W. F., Chesley, S. R., Scheeres, D. J., & Statler, T. S. 2015, Asteroids IV (Tucson, AZ: Univ. Arizona Press), 509
Vokrouhlický, D., & Milani, A. 2000, A&A, 362, 746
Walsh, K. J., Morbidelli, A., Raymond, S. N., O'Brien, D. P., & Mandell, A. M. 2011, Natur, 475, 206
Wang, J. H., & Brasser, R. 2014, A&A, 563, A122
Williams, G. V., Sato, H., Sarneczky, K., et al. 2017, CBET, 4450, 1
Wright, E. L., Masiero, J., & Mainzer, A. 2021, in 7th IAA Planetary Defense Conf. (Vienna: IAA), 242
Ye, Q.-Z., Zhang, Q., Kelley, M. S. P., & Brown, P. G. 2017, ApJL, 851, L5